Ultrasonic Activation of Au_{144}/TiO_2: Tuning Hydroxyl Radical Production through Frequency and Nanocluster Size

Takaaki Tsurunishi , Yuzuki Furui , Hideya Kawasaki *

Posted Date: 10 December 2024

doi: 10.20944/preprints202412.0815.v1

Keywords: sonocatalyst; TiO2; Au nanoclusters; reactive oxygen species; ultrasonic cavitation

Article

Ultrasonic Activation of Au_{144}/TiO_2: Tuning Hydroxyl Radical Production Through Frequency and Nanocluster Size

Takaaki Tsurunishi, Yuzuki Furui and Hideya Kawasaki *

Department of Chemistry and Materials Engineering, Kansai University, 3-3-35, Yamate-cho, Suita, Osaka 564−8680, Japan

* Correspondence: hkawa@kansai-u.ac.jp

Abstract: This study explores the sonocatalytic activity of gold nanoclusters (Au NCs) combined with titanium dioxide (TiO_2) nanoparticles, forming Au_{144}/TiO_2 composites. The hybrid material significantly enhances hydroxyl radical (•OH) generation under ultrasonic conditions, attributed to high-energy cavitation bubbles formed during ultrasonication. The effects of frequency (200, 430, and 950 kHz) and power were systematically evaluated, identifying 430 kHz as optimal for •OH production due to its efficient cavitation energy. Au_{144} NCs function as electron traps, reducing electron–hole recombination in ultrasonically activated TiO_2, thereby improving charge separation and enhancing •OH generation. Size-dependent effects were also studied, showing an efficiency trend of Au_{144} > Au_{25} > plasmonic Au nanoparticles > bare TiO_2. These findings highlight the importance of ultrasonication frequency and Au NC size in optimizing sonocatalytic performance, providing valuable insights for designing advanced sonocatalysts with applications in chemical synthesis, environmental remediation, and biomedical fields.

Keywords: sonocatalyst; TiO_2; Au nanoclusters; reactive oxygen species; ultrasonic cavitation

1. Introduction

The hydroxyl radical (•OH) is an exceptionally potent oxidizing agent found in various environments, including natural waters, the atmosphere, and interstellar space. As one of the most important reactive oxygen species (ROS), •OH plays a pivotal role in numerous chemical processes, particularly in environmental chemistry and biochemistry. In environmental applications, advanced oxidation processes (AOPs) are widely employed in wastewater treatment to degrade pollutants effectively [1,2]. In the medical field, •OH radicals are utilized in innovative therapeutic approaches such as photodynamic therapy and chemodynamic therapy, which target cancer cells through oxidative damage within the tumor microenvironment [3,4]. Advancing methods for enhanced •OH radical generation is critical for expanding its potential applications in both environmental remediation and healthcare.

Photocatalytic materials absorb light with energy exceeding their band gap, generating excited electrons and holes. These charge carriers migrate to the surface of the material, where they act as reducing and oxidizing agents, facilitating redox reactions. For example, the reduction of oxygen or the oxidation of water results in the formation of reactive oxygen species (ROS), such as superoxide radicals and •OH. These ROS play a key role in degrading organic compounds. However, a significant portion of the excited electrons and holes recombine before contributing to the reaction, releasing energy as heat instead [5,6].

In addition to photocatalysis, sonocatalysis involves the activation of materials, known as sonocatalysts, by ultrasound waves in liquids through high-energy acoustic cavitation. The collapse of cavitation bubbles generates extreme heat and pressure, causing the pyrolytic cleavage of water molecules. This process thermally dissociates water into •OH and hydrogen atoms, often accompanied by sonoluminescence. The effectiveness of sonocatalysts arises from the inherent

 doi:10.20944/preprints202412.0815.v1

sonocatalytic activity of semiconductors [6,7]. In the medical field, sonocatalysts are pivotal in sonodynamic therapy, where ultrasound activates the sonocatalysts to produce ROS, selectively destroying tumor cells. Thus, sonocatalysts play a vital role in tackling environmental challenges and advancing medical therapies [8,9].

Sonocatalysts, primarily composed of metals or metal oxides, are widely utilized in environmental remediation and therapeutic applications to facilitate chemical reactions and degrade persistent contaminants. Among these materials, titanium dioxide (TiO_2) is one of the most extensively studied in sonocatalysis [6,7,10,11]. Recent research has aimed to enhance the efficiency of TiO_2-based sonocatalytic processes and expand their applications in both medical and environmental fields [12–18]. Incorporating TiO_2 nanoparticles (NPs) with noble metals, such as gold (Au), has been shown to improve their sonocatalytic performance [19–21]. Noble metals not only extend the absorption spectrum through surface plasmon resonance but also serve as electron sinks, facilitating electron transfer and reducing electron-hole recombination.

Gold nanoclusters (Au NCs), tiny aggregates of Au atoms with diameters smaller than 2 nm, exhibit unique properties distinct from bulk gold and larger plasmonic Au NPs [22–24]. These clusters display unique electronic states due to quantum-size effects. Structurally, Au NCs consist of a gold atom core surrounded by a protective layer of organic ligands. Their electronic structures, characterized by specific energy levels such as the highest occupied molecular orbital (HOMO) and lowest unoccupied molecular orbital (LUMO), vary with cluster size and significantly influence their physicochemical properties. As innovative nanomaterials, Au NCs hold great potential in catalysis and luminescence, primarily due to their size-dependent properties and exceptional stability [25–27].

In our previous research, we explored the sonocatalytic potential of Au NCs [28,29]. Specifically, we synthesized Au_{144} NCs /TiO_2 composites by integrating Au_{144} NCs with TiO_2 NPs. The composites exhibited significantly enhanced sonocatalytic activity compared to TiO_2 alone under ultrasonication at 1 MHz [30]. The sonocatalytic activation of the Au_{144}/TiO_2 composite is primarily driven by the generation of high-energy cavitation bubbles during ultrasonication. The characteristics of these cavitation bubbles, which are influenced by the power and frequency of ultrasonication, play a crucial role in determining the sonocatalytic performance of the composite. Despite the promising results, the current literature provides limited insight into how ultrasonication frequency and power affect the sonocatalytic efficiency of Au NCs/TiO_2-based catalysts. To address this gap, our ongoing research aims to optimize the sonocatalytic performance of Au_{144}/TiO_2 composites by systematically refining ultrasonic irradiation parameters, including frequency, intensity, and catalyst concentration. By identifying the optimal conditions for ultrasonic catalysis, we aim to maximize the efficiency of the composites. Additionally, we investigated the size-dependent effects of Au NCs (including plasmonic Au NPs) on the performance of Au NCs/TiO_2-based catalysts. Specifically, we compared Au_{144} NCs, Au_{25} NCs, and plasmonic Au NPs. These findings have the potential to broaden the application of these advanced sonocatalytic materials in diverse industrial and environmental contexts.

2. Results and Discussion

2.1. Preparation of Au_{144}/ TiO_2 Nanocomposite

The Au_{144}/TiO_2 nanocomposite was prepared by adsorbing Au_{144} NCs onto TiO_2 NPs. The UV-Vis absorption spectrum of the $Au_{144}(pMBA)_{60}$ NCs exhibited a peak at 280 nm, corresponding to 4–mercaptobenzoic acid (pMBA), along with a broad peak at 520 nm, as shown in **Figure 1a**. These spectral features are consistent with previously reported characteristics of $Au_{144}(pMBA)_{60}$ [30,31]. TEM analysis confirmed that the Au_{144} NCs, comprising 3 wt.%, were successfully loaded onto the TiO_2 NPs without signs of aggregation. The observed particle size was less than 2 nm (**Figure 1b**). The reflectance spectra of Au_{144} NCs (3.0 wt.%)/TiO_2 were evaluated using the Kubelka-Munk (K-M) function, as shown in Figure 1c. This analysis demonstrated UV-vis absorption attributed to the loaded Au_{144} NCs, which was notably absent in pristine TiO_2. Additionally, X-ray fluorescence (XRF)

 doi:10.20944/preprints202412.0815.v1

measurements conducted on the Au_{144} NCs (3.0 wt.%)/TiO_2 powder samples determined the gold content to be 2.6 ± 0.2 wt.% (Figure 1d).

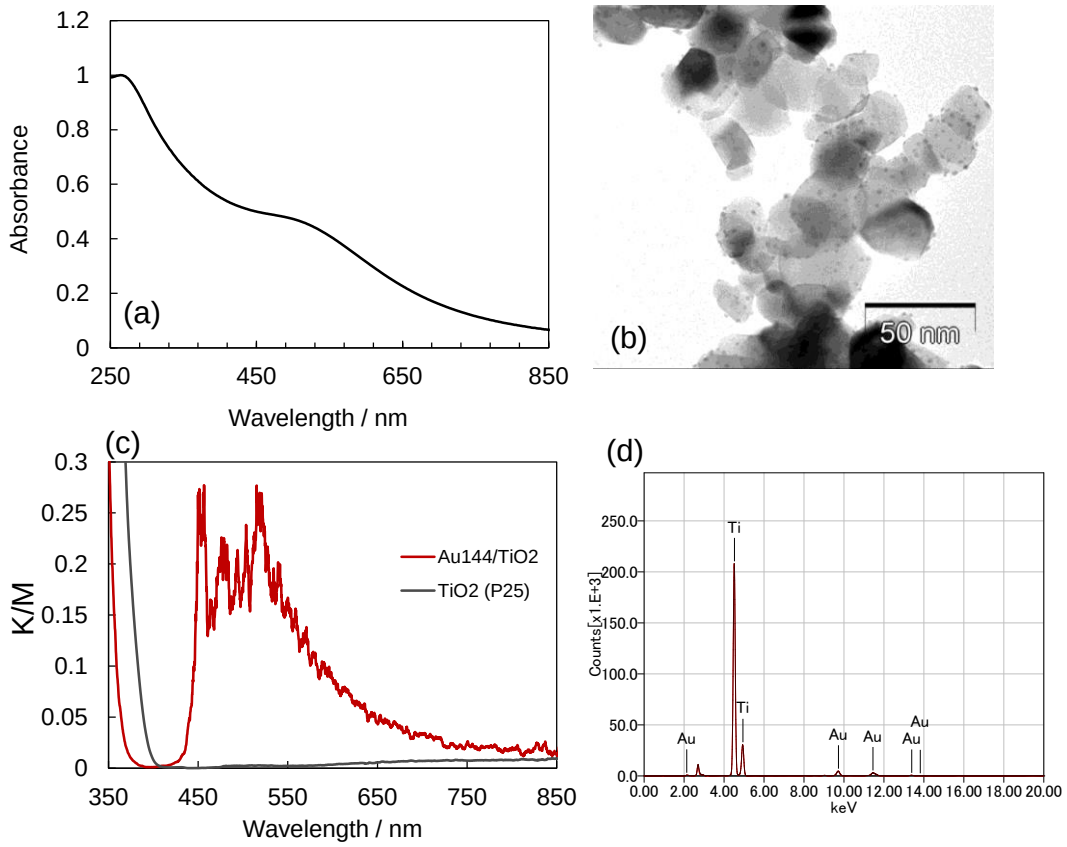

Figure 1. (a) UV-Vis absorption spectrum of Au_{144} NCs. (b) TEM image of $Au1_{44}$ (3 wt.%)/TiO_2.(c) Absorption spectrum of Au144 (3 wt.%)/TiO_2. (d) XRF spectrum of Au_{144} NCs (3 wt.%)/TiO_2.

2.2. Sonocatalysis of TiO_2 vs Au_{144}/TiO_2

When ultrasound was applied to a reaction solution containing the Au_{144}/TiO_2 sonocatalyst, two primary pathways for the generation of •OH radicals were identified: (i) thermal cleavage of water at localized hot spots, and (ii) water oxidation facilitated by the ultrasonically excited sonocatalysts [6–9]. To evaluate the sonocatalyst's ability to produce •OH radicals, we measured the fluorescence intensity increase at 425 nm in a disodium terephthalate(NaTA) solution under ultrasonic conditions at 430 kHz and 5 W, both with and without the sonocatalyst. The presence of •OH radicals was detected using NaTA, which reacts with •OH radicals to form fluorescent 2-hydroxy disodium terephthalate (HTA)[30]. The observed increase in fluorescence intensity in the catalyst-containing reaction solution (ΔPL_t) was compared to that in the absence of the catalyst (ΔPL_0). The difference, $\Delta Int_{sono} = \Delta PL_t - \Delta PL_0$, represents the net contribution of the sonocatalyst to •OH radical generation. This parameter, ΔInt_{sono}, is depicted in **Figures 2a and 2b** and serves as a quantitative indicator of sonocatalytic activity. The fluorescence intensity increase in the presence of Au_{144}/TiO_2 was higher than that observed for TiO_2 alone. This finding demonstrates that the deposition of Au_{144} NCs onto TiO_2 NPs enhances the sonocatalytic activity, particularly in the generation of •OH radicals.

 doi:10.20944/preprints202412.0815.v1

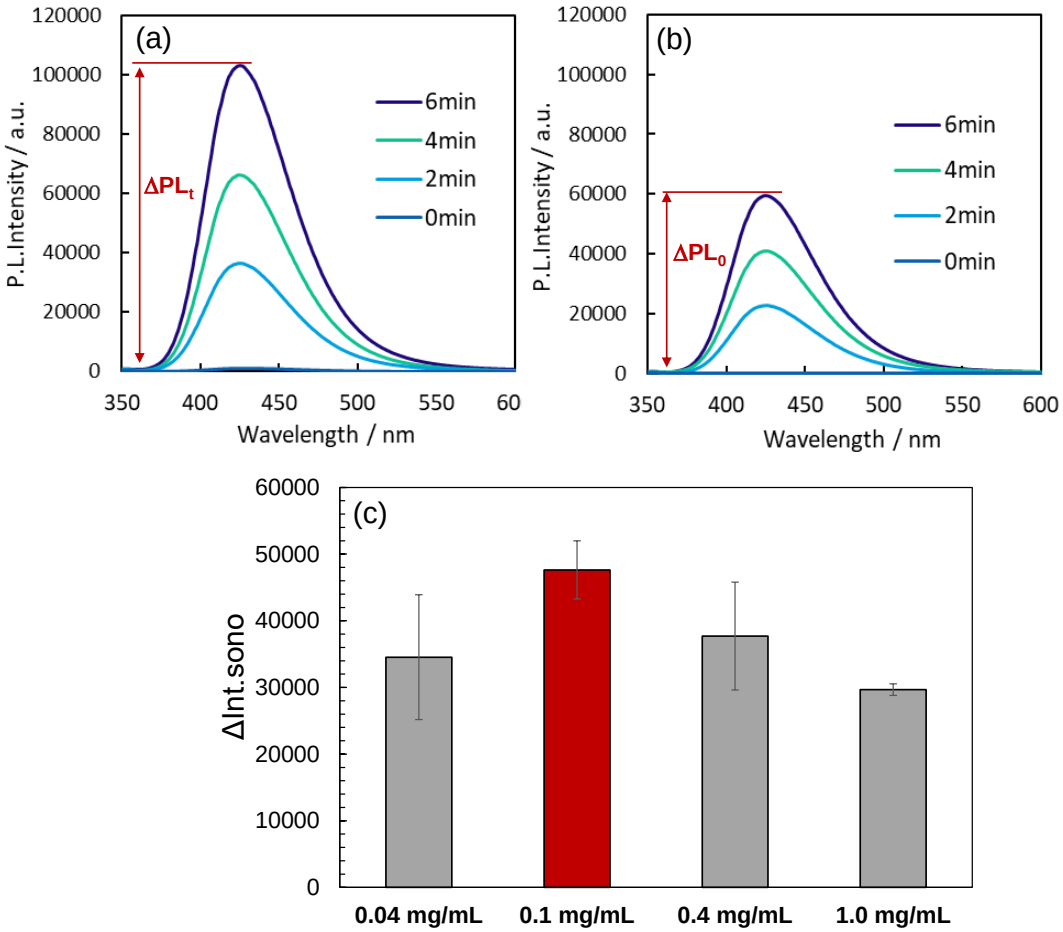

Figure 2. Fluorescence spectra of a NaTA solution during ultrasonic irradiation for 6 min at 430 kHz and 5 W, with (a) Au_{144} NCs (3 wt.%)/TiO_2, and (b) TiO_2 alone. Catalyst concentration: 0.1 mg/mL. (c) Fluorescence intensity increase (ΔInt_{sono}) at 425 nm after 6 min of ultrasonic irradiation with varying concentrations of Au_{144} NCs (3 wt.%)/TiO_2: 0.04 mg/mL, 0.1 mg/mL, 0.4 mg/mL, and 1.0 mg/mL.

Catalyst Concentration Dependence: Understanding the dependence of sonocatalytic activity on catalyst concentration is critical for optimizing reaction conditions. An appropriate catalyst concentration ensures maximum •OH radical generation while avoiding potential drawbacks such as light scattering or shielding effects that can occur at higher concentrations. To identify the optimal concentration for the Au_{144}/TiO_2 catalyst, we evaluated its performance at varying concentrations.

We measured ΔPLt over a 6-minute period of ultrasonic irradiation at a frequency of 430 kHz and an intensity of 5.0 W on reaction solutions containing different concentrations of Au_{144}/TiO_2 (0.04, 0.1, 0.4, and 1.0 mg/mL). Plots of ΔInt_{sono} over the 6-minute duration of irradiation are presented in **Figure 2c.** Across all reaction solutions, a notable increase in ΔInt_{sono} was observed, indicating the oxidation of NaTA to HTA, accompanied by the generation of •OH radicals via Au_{144}/TiO_2. The ΔInt_{sono} values followed the order: 0.1 mg/mL > 0.4 mg/mL > 0.04 mg/mL > 1.0 mg/mL, suggesting that the catalytic activity is maximized at a concentration of 0.1 mg/mL. This behavior may be explained by the mechanism of sonocatalyst photoexcitation via sonoluminescence light absorption[32]. At optimal concentrations, the catalyst efficiently absorbs sonoluminescence light, resulting in enhanced •OH radical generation. However, at excessive concentrations, the catalyst may block the sonoluminescence light, limiting the excitation to catalyst particles near the sonoluminescence source. Consequently, the ability to generate •OH radicals decreases as the concentration increases beyond 0.4 mg/mL. Based on these findings, the optimal concentration of the Au_{144}/TiO_2 catalyst was determined to be 0.1 mg/mL, and this concentration was maintained for all subsequent experiments to ensure maximum sonocatalytic activity.

 doi:10.20944/preprints202412.0815.v1

3.3. Ultrasound Frequency and Power Dependence

The efficiency of sonocatalytic reactions is highly dependent on ultrasonic frequency and power, as these parameters directly influence the generation and collapse of cavitation bubbles. The cavitation dynamics vary with frequency and power, affecting the energy distribution and localized conditions at cavitation hotspots [6–9]. Understanding the optimal frequency and power for the Au_{144}/TiO_2 sonocatalyst is crucial for maximizing •OH radical production and ensuring efficient sonocatalytic performance. Furthermore, investigating these parameters provides insight into the mechanisms of ultrasonic activation and the role of cavitation in sonocatalysis.

Ultrasound Frequency Dependence: We investigated the influence of ultrasonic frequencies on ΔIntsono at 200 kHz, 430 kHz, and 950 kHz, as shown in **Figure 3a**. For all reaction solutions containing Au_{144}/TiO_2, the ΔInt_{sono} values were consistently higher than those of pristine TiO_2. The observed effect of ultrasonic frequency on enhanced sonocatalytic activity followed the order: 430 kHz > 200 kHz > 950 kHz. This trend indicates that the generation rate of •OH radicals was maximized at 430 kHz, driven by the superior sonocatalytic performance of the Au_{144}/TiO_2 catalyst.The frequency dependence can be attributed to variations in cavitation and sonoluminescence efficiency at different frequencies. Cavitation bubbles, formed under ultrasonic irradiation, collapse to produce extreme localized temperatures and pressures, facilitating water pyrolysis and the production of •OH radicals. Measurements of •OH radical production using NaTA aqueous solutions without a catalyst revealed higher bubble temperatures at 430 kHz compared to 200 kHz and 950 kHz (**Figure 4a**). At 430 kHz, the amount of •OH radicals increased in correlation with the ultrasonic intensity(**Figure 4b**).This finding suggests that water pyrolysis, and consequently •OH radical generation, was most effective at 430 kHz.Previous studies have reported that sonoluminescence intensity peaks at intermediate frequencies, such as 358 kHz, but declines at higher frequencies, such as 1071 kHz [33,34]. This behavior supports the conclusion that the efficient ultrasonic excitation of the Au_{144}/TiO_2 catalyst at 430 kHz arises from the combined thermal effects and sonoluminescence induced by cavitation hotspots. These results emphasize the pivotal role of cavitation dynamics in activating the Au_{144}/TiO_2 catalyst and enhancing its sonocatalytic efficiency.

Power Dependence of Sonocatalytic Activity: To further evaluate the impact of ultrasonic power on sonocatalytic performance, we analyzed ΔInt_{sono} at 430 kHz with power levels of 1.0 W, 3.0 W, and 5.0 W, as shown in **Figure 3b**. The results revealed a power-dependent increase in ΔInt_{sono}, following the order: 5.0 W > 3.0 W > 1.0 W. However, power levels exceeding 5 W did not significantly enhance ΔInt_{sono} and posed risks of equipment damage, such as deterioration of the ultrasonic transmission gel. These observations suggest that 5.0 W represents an optimal power level, balancing effective •OH radical generation with equipment safety. At lower power levels, insufficient cavitation activity limits radical production, while excessively high power levels may lead to inefficiencies caused by energy dissipation or hardware constraints.

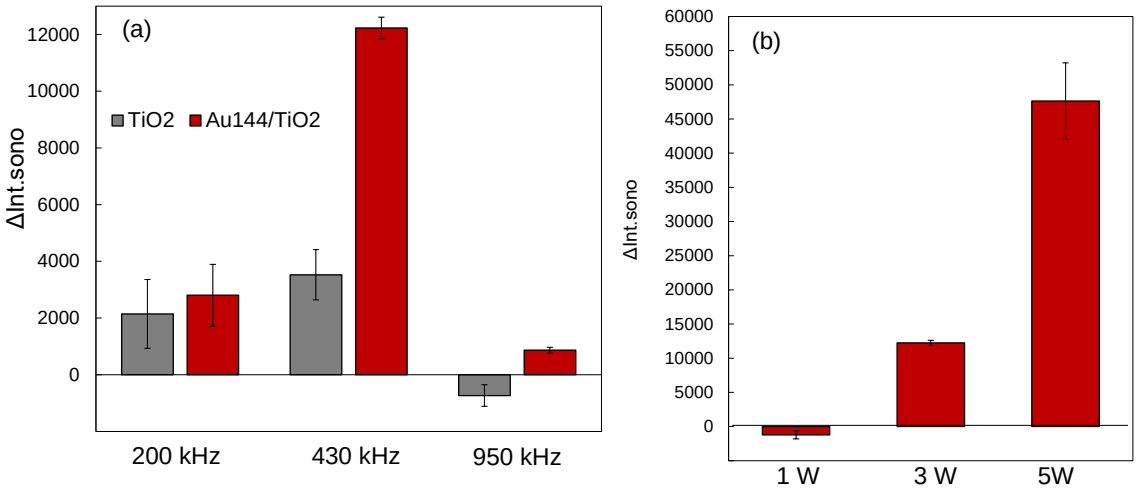

 doi:10.20944/preprints202412.0815.v1

Figure 3. (a) Fluorescence intensity increase (ΔIntsono) at 425 nm after ultrasonic irradiation at 3 W for 6 min with TiO_2 alone and Au_{144} (3 wt.%)/TiO_2 at different ultrasonic frequencies: 200 kHz, 430 kHz, and 950 KHz. Catalyst concentration: 0.1 mg/mL. (b) Fluorescence intensity increase (ΔIntsono) at 425 nm after ultrasonic irradiation at 430 kHz for 6 min with Au_{144} (3 wt.%)/TiO_2 at varying ultrasonic power levels: 1 W, 3 W, and 5 W. Catalyst concentration: 0.1 mg/mL.

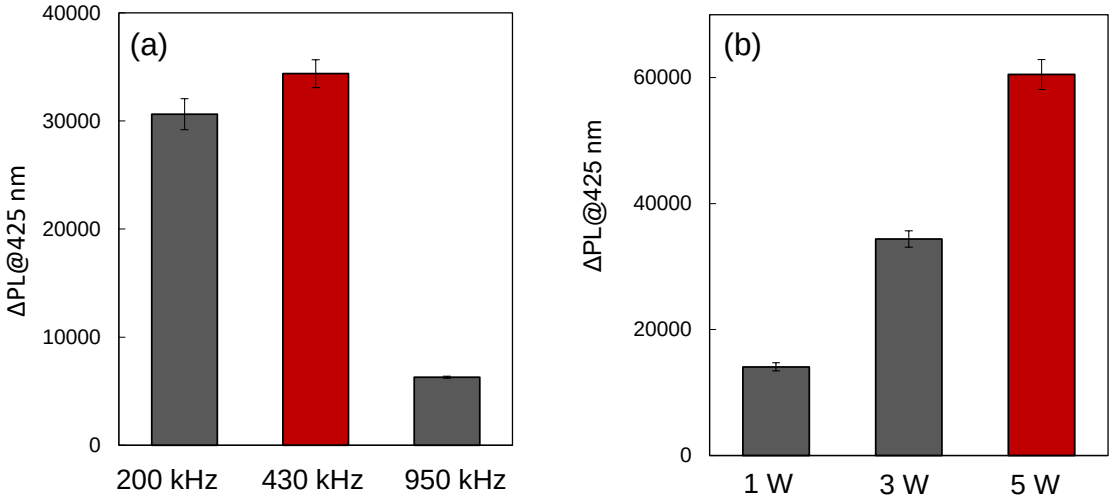

Figure 4. (a) Fluorescence intensity increase (ΔPL) of NaTA aqueous solutions (no catalyst) at 425 nm after 6 min of ultrasonic irradiation at 3 W, with varying the ultrasonic frequencies of 200 kH, 430 kHz, and 950 kHz. (b) Fluorescence intensity increase (ΔPL) of NaTA aqueous solutions (no catalyst) at 425 nm after 6 min of ultrasonic irradiation at 450 kHz with varying the ultrasonic power of 1W, 3W and 5 W.

3.4. Mechanistic Insights into Enhanced Sonocatalytic Activity in Au_{144}/TiO_2

The enhanced sonocatalytic activity of Au_{144}/TiO_2 at 430 kHz compared to TiO_2 alone demonstrates the enhanced effects of Au_{144} NCs deposited on TiO_2. **Figure 5** illustrates the mechanisms driving enhanced •OH radical generation in the Au_{144}/TiO_2 sonocatalyst system under ultrasonic irradiation. This model highlights two key processes: ultrasonic cavitation-induced excitation and charge separation, which together contribute to the system's superior sonocatalytic performance. During ultrasonic irradiation, acoustic pressure cycles lead to the formation, growth, and collapse of cavitation bubbles, as depicted in **Figure 5a.** The collapse of these bubbles creates extreme localized conditions, such as transiently high temperatures and pressures at cavitation hot spots. These conditions induce thermal effects and the UV sonoluminescence in the wavelength range of 200–400nm [32], which promote the excitation of electrons in TiO_2 from the valence band (VB) to the conduction band (CB). The excited electrons are subsequently transferred to the Au_{144} NCs. This efficient electron migration suppresses electron-hole recombination, thereby prolonging the lifetime of charge carriers. The enhanced charge separation facilitates more effective water oxidation, increasing the production of •OH radicals, as depicted in **Figure5b**.

Preprints.org (www.preprints.org) | NOT PEER-REVIEWED | Posted: 10 December 2024 doi:10.20944/preprints202412.0815.v1

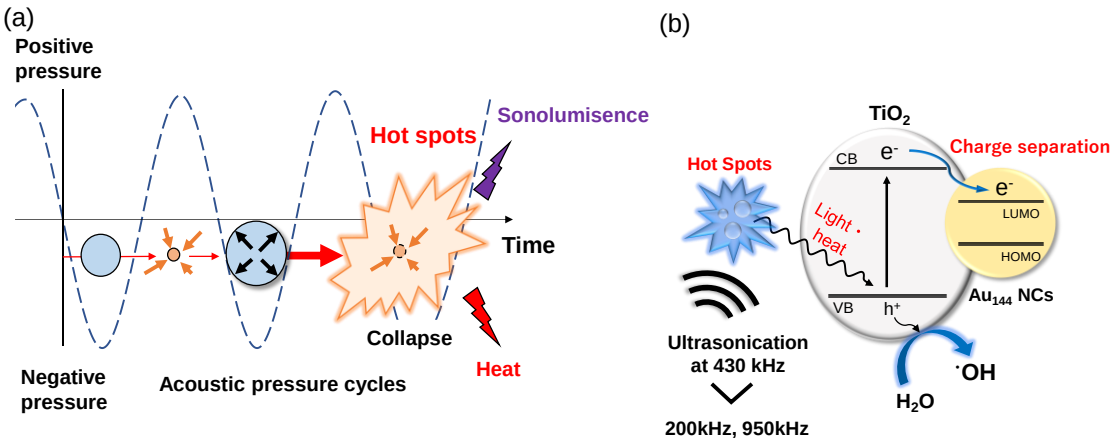

Figure 5. Conceptual diagram illustrating enhanced •OH radical generation in Au_{144} NCs /TiO_2 sonocatalyst system. (a) Thermal and sonoluminescence generation at cavitation hot spots during ultrasonication. (b) Enhanced mechanism for •OH radical generation involving the migration of excited electrons from TiO_2 to Au_{144} NCs, simultaneously inhibiting electron-hole recombination.

To validate this hypothesis, transient photocurrent and sonocurrent measurements were conducted for Au_{144}/TiO_2 composites and bare TiO_2. Transient photocurrent and sonocurrent measurements serve as direct experimental evidence for enhanced charge separation in photocatalytic and sonocatalytic systems. A higher photocurrent or sonocurrent indicates more efficient charge carrier generation and reduced recombination of electron-hole pairs. These measurements are thus widely used to evaluate the ability of a material to facilitate charge separation under irradiation or ultrasonic excitation [35]. As shown in **Figure 6a**, Au_{144}/TiO_2 exhibited a significantly higher photocurrent density under light exposure compared to bare TiO_2, indicating improved charge separation and transfer. Similarly, transient sonocurrent measurements at 430 kHz (**Figure 5b**) demonstrated enhanced electron generation in Au_{144}/TiO_2 compared to TiO_2 alone. These findings provide strong evidence that Au_{144} NCs play a crucial role in facilitating charge separation and improving the overall sonocatalytic performance of the system.

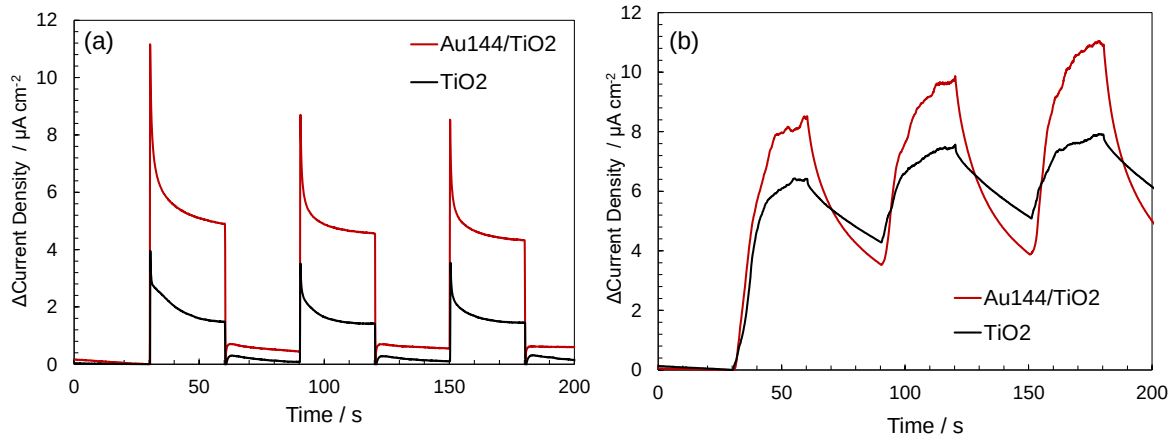

Figure 6. (a) Transient photocurrent profile, and (b) transient sonocurrent profile comparison between TiO_2 and Au_{144}(3 wt%) /TiO_2.

3.5. Size Dependence in Sonocatalytic Activity in Au/TiO₂

Understanding the size-dependent effects of Au NCs is crucial for optimizing TiO_2-based catalytic systems, particularly in addressing charge separation challenges. This study examines how the size of Au NCs influences the sonocatalytic performance of Au/TiO_2 catalysts. The catalytic efficiency of variously sized Au NCs, including plasmonic Au nanoparticles (NPs), was evaluated

 doi:10.20944/preprints202412.0815.v1

(**Figure 7**). The ΔInt_{sono} values, which represent sonocatalytic efficiency, followed the order: Au_{144} > Au_{25} > plasmonic Au NPs > bare TiO_2. These findings highlight the superior performance of Au NCs compared to plasmonic Au NPs within the Au/TiO_2 catalyst system.

Among the studied catalysts, Au_{144} NCs exhibited the highest performance, outperforming Au_{25} NCs by achieving an optimal balance between electron migration and charge separation. Smaller clusters, such as Au_{25} NCs, are known to inject photoexcited electrons into the TiO_2 conduction band upon light absorption [36]. However, this bidirectional electron transfer between Au_{25} NCs and TiO_2 increases the frequency of charge recombination events, potentially reducing the efficiency of sonocatalytic reactions. In contrast, ultra-small Au NCs (< 2 nm) possess exceptionally high surface energy at the atomic level, significantly enhancing their catalytic activity. Larger Au NPs (~2.4 nm), with a relatively reduced reactive surface area, demonstrate diminished catalytic performance.

The transition from Au NCs to plasmonic Au NPs, as well as the size-dependent effects and electronic structure variations, remains only partially understood. Future research should focus on elucidating the interplay between size and electronic structure using advanced spectroscopy and computational modeling. These insights will deepen our understanding of Au-based catalytic systems, emphasizing the critical role of Au NC size and electronic structure in enhancing sonocatalytic performance..

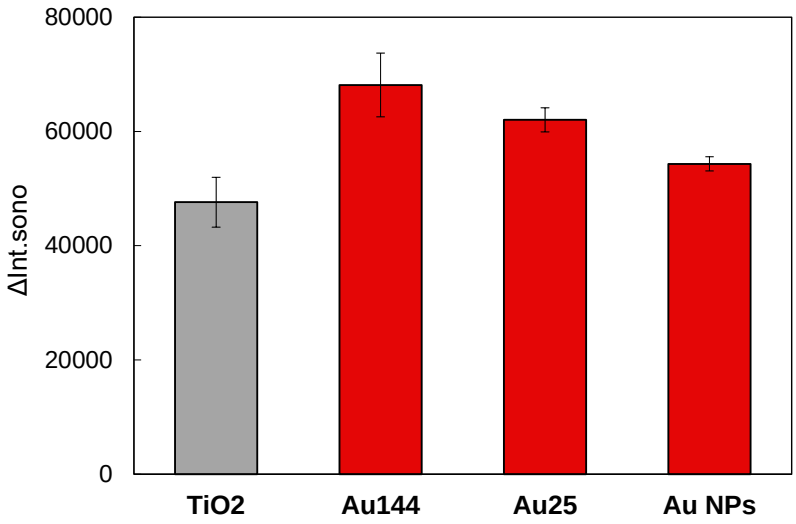

Figure 7. Fluorescence intensity increase (ΔInt_{sono}) at 425 nm after ultrasonic irradiation at 5 W for 6 min with TiO_2 alone and Au (3 wt.%)/TiO_2 at an ultrasonic frequency of 430 kHz. Catalyst concentration: 0.1 mg/mL.

3. Materials and Methods

3.1. Reagents

Hydrogen tetrachloroaurate (III) tetrahydrate ($HAuCl_4 \cdot 4H_2O$), and methanol were sourced from FUJIFILM Wako Pure Chemical Corporation. Disodium terephthalate (NaTA) and 4–mercaptobenzoic acid (pMBA) were purchased from Tokyo Chemical Industry Co. Ltd. Sodium borohydride (99%) ($NaBH_4$) was procured from Sigma–Aldrich. The TiO2 utilized was Aeroxide®P25. Deionized water was prepared using a water distillation apparatus (Aquarius RFD250; ADVANTEC).

3.2. Instruments

UV-visible (UV-vis) absorption spectroscopy and steady-state fluorescence spectroscopy were performed using a JASCO V-670 spectrophotometer (JASCO Corp., Japan) and RF-6000 spectrofluorometer (Shimadzu Corp., Japan), respectively. Diffuse reflectance UV-vis spectra were acquired using an Ocean Optics DH-2000-BAL deuterium-tungsten-halogen light source and an Ocean Optics USB4000 compact fiber optic spectrometer (Ocean Optics, Dunedin, FL, USA). The Au

 doi:10.20944/preprints202412.0815.v1

loading on TiO2 NPs was quantified using an energy-dispersive X-ray fluorescence (XRF) spectrometer (JSX-1000S Element Eye; JEOL Ltd., Japan). The crystal structure of the TiO_2 NPs powder was analyzed by X-ray diffractometry (XRD, D2 Phaser, Bruker AXS GmbH, Karlsruhe, Germany), employing a Cu-Kα radiation source (λ = 1.5406 Å) over a 2θ range of 10–80°, at an accelerating voltage of 30 kV and a current of 10 mA. The size and morphology of Au144/TiO2 were characterized using transmission electron microscopy (TEM; JEOL JEM2100 microscope operating at 200 kV).

3.3. Synthesis of $Au_{144}(pMBA)_{60}$

According to our previous study [30,31], $Au_{144}(pMBA)_{60}$ NCs (Au_{144} NCs) were synthesized at an ambient temperature by mixing HAuCl4 aqueous solution (25 mM, 3 mL), pMBA solution (75 mM, 3 mL), deionized water (6.5 mL), and methanol (12.5 mL), with methanol comprising 50% of the total volume of 25 mL. After stirring the solution overnight until it turned colorless, NaBH4 was added in cold deionized water (500 mM, 227 µL), and the mixture was stirred for an additional 2 h. After the addition of methanol, the NCs were isolated by centrifugation, and the purification step was repeated. Finally, the NCs were dried under reduced pressure to obtain the purified product.

3.4. Synthesis of $Au_{25}(pMBA)_{18}$

The synthesis of $Au_{25}(pMBA)_{18}$ nanoclusters (Au_{25} NCs) was conducted at room temperature in air, following a previously reported method [30]. The successful synthesis of $Au_{25}(pMBA)_{18}$ was confirmed through UV–vis spectroscopy, which revealed two prominent absorption bands at 450 nm and 670 nm, along with a broad shoulder around 800 nm. These spectral features align well with previously reported characteristics of Au_{25} NCs [30].

3.5. Synthesis of Au Nanoparticles

Gold nanoparticles (Au NPs) with a size of 2.4 nm were synthesized under ambient conditions and at room temperature following the reported procedure [37]. Initially, 2.7 mL of the 28 mM $HAuCl_4$ solution and 2.4 mL of the 95 mM pMBA solution were mixed. This was followed by the gradual addition of 20 mL of the 106 mM NaOH solution. The resulting reaction mixture was stirred continuously for 20 hours to ensure complete interaction of the components. The final concentrations of the key reactants in the reaction mixture were as follows: $HAuCl_4$, 3 mM; pMBA, 9 mM; and NaOH, 100 mM. To reduce the gold ions, 28.3 mg of $NaBH_4$ was dissolved in 5 mL of cold deionized water, yielding a 150 mM $NaBH_4$ solution. Subsequently, a 0.25 mL aliquot of this $NaBH_4$ solution was added to the reaction mixture, maintaining a molar ratio of $NaBH_4$:Au = 1:2. The reaction was stirred overnight to facilitate reduction. To complete the synthesis, 29.2 mg of NaCl was added to the reaction mixture to achieve a final NaCl concentration of 10 mM. Methanol (80% v/v) was then introduced, and the mixture was centrifuged at 6000 rpm for 10 minutes. The resulting precipitate was collected, dried, and stored, yielding the final Au NPs. The successful synthesis of Au NPs was confirmed through UV–vis spectroscopy, which revealed a plasmonic absorption band at around 520 nm [37].

3.6. Preparation of Au /TiO_2 Composites

Following the method described in our previous report [30], a Au_{144} NCs-supported TiO_2 composite was fabricated at ambient temperature. In a reaction tube, 8 mL of an aqueous TiO_2 dispersion (1 mg/mL) was combined with 80 µL of an aqueous Au144 NC solution (3.0 mg/mL). The mixture was stirred at 800 rpm for 17 hours to promote the adsorption of Au_{144} NCs onto the TiO_2 particles, yielding a composite with a 3 wt.% loading of Au_{144} NCs on TiO_2. After stirring, the mixture was centrifuged at 6000 rpm for 15 minutes to separate the supernatant, leaving the Au_{144} NCs (3 wt.%)/TiO_2 composite as a precipitate. Similarly, composites of Au_{25} NCs (3 wt.%) and Au NPs(3 wt.%) supported on TiO_2 were prepared using the same procedure.

 doi:10.20944/preprints202412.0815.v1

3.7. Evaluation of Sonocatalytic Activity

The sonocatalytic activity of Au /TiO_2 nanocomposites was assessed by measuring the generation of •OH radicals from water under ultrasonic stimulation. The presence of •OH radicals was detected using sodium terephthalate (NaTA), which reacts with •OH radicals to form fluorescent 2-hydroxy disodium terephthalate (HTA)[30]. The production of •OH radicals was monitored by measuring the fluorescence intensity of HTA at 425 nm (excitation at 315 nm). To ensure consistent ultrasonic transmission and eliminate air gaps, an ultrasonic transmission gel was applied between the transducer and a plastic dish during the experiment. The experimental setup was maintained at a constant temperature of 18 ± 2 °C using a temperature-controlled water bath equipped with a precision thermostat. The reaction solution was subjected to ultrasonic irradiation at intervals of 0, 2, 4, and 6 minutes using a QUAVA Mini QR-003 ultrasonic device at frequencies of 200 kHz, 430 kHz, and 930 kHz. After each irradiation, the mixture was centrifuged at 14,000 rpm for 10 minutes to separate the catalyst. The fluorescence intensity of the supernatant was measured at 425 nm to quantify the production of •OH radicals.

3.8. Transient Photocurrent/Sonocurrent Measuremetns in TiO_2 and Au_{144}(3 wt%) /TiO_2.

To determine whether supporting Au_{144} NCs on TiO_2 improves charge separation, transient photocurrent and ultrasonic current responses were measured using a three-electrode cell connected to a potentiostat (BAS, ALS611 DE). The measurement parameters were as follows: mode—Amperometry i-t Curve; initial potential—-0.1 V; sample interval—0.1 s. A Pt mesh served as the counter electrode, and an Ag/AgCl electrode (BAS, RE-1B) was used as the reference electrode. The working electrode was prepared by dispersing 5 mg of the catalyst in a mixture of 375 μL of water containing 20 wt.% Nafion (50 μL) and 125 μL of 2-propanol. A 40 μL aliquot of this dispersion was applied onto a 1 cm^2 fluorine-doped tin oxide (FTO) glass conductive surface and dried under reduced pressure overnight.

All measurements were performed in a 0.2 M Na_2SO_4 aqueous solution. The transient photocurrent response was recorded under UV light (394 nm, 22.46 mW/cm^2) using a UV Spotlight Source (L5662, Hamamatsu Photonics). For the transient ultrasonic current response, a 200 kHz, 50 W ultrasound device (QUAVA mini QR-003, Kaijo Corporation) was employed. To minimize temperature elevation in the electrolyte due to ultrasonic irradiation, the reaction vessel was placed on a cooling plate submerged in a water-filled container

4. Conclusion

In this study, we investigated the sonocatalytic capabilities of Au_{144}/TiO_2 composites, focusing on the generation of •OH radicals under varying ultrasonic frequencies, power levels, and NC sizes. Our findings demonstrate that the Au_{144}/TiO_2 composite exhibits superior sonocatalytic performance, particularly at an ultrasonic frequency of 430 kHz and a power setting of 5.0 W. This heightened activity is attributed to the optimal cavitation dynamics achieved at 430 kHz, which maximizes localized thermal effects and sonoluminescence, facilitating efficient •OH radical generation.

The size dependence of the Au NCs was also found to play a critical role in determining the sonocatalytic performance in Au/TiO_2 composites. The comparative analysis revealed a clear efficiency trend: Au_{144} > Au_{25} > plasmonic Au NPs > bare TiO_2. Larger clusters like Au_{144} demonstrated superior activity due to their discrete electronic structures, which enable better energy alignment with the TiO_2 conduction band, facilitating enhanced charge separation and prolonged carrier lifetimes. In contrast, plasmonic Au NPs were less efficient under ultrasonic activation.

This research highlights the practical potential of the Au_{144}/TiO_2 system for applications in environmental remediation and medical treatments. The insights gained into the interplay between ultrasonic frequency, cavitation dynamics, and nanocluster size offer a pathway for developing advanced sonocatalytic materials. Ultimately, this study contributes to the broader field of chemical physics by emphasizing the significance of NP-enhanced sonocatalysis in addressing global challenges, including pollution control and sustainable healthcare solutions.

Author Contributions: Conceptualization: Hideya Kawasaki formulated the overarching research goals and aims, while Takaaki Tsurunishi framed the specific hypotheses to be tested;Methodology: Takaaki Tsurunishi and Yuzuki Furui designed the experimental and analytical processes; Investigation: Takaaki Tsurunishi conducted the primary experiments and data collection; Writing – Original Draft Preparation: Takaaki Tsurunishi drafted the manuscript; Writing – Review & Editing: Hideya Kawasaki provided critical review, commentary, and revisions to the manuscript;Visualization: Takaaki Tsurunishi created all diagrams and visual aids that helped to interpret data; Supervision: Hideya Kawasaki oversaw the project, including coordination and strategic guidance; Project Administration: Hideya Kawasaki managed the project administration, including compliance with funding and ethical requireme

Funding: This work was supported by JSPS KAKENHI (Grant No. JP 22H01915) and Kansai University Fund for Supporting formation of strategic Research Centers(University initiative type).

Institutional Review Board Statement: Not applicable.

Informed Consent Statement: Not applicable.

Data Availability Statement: Data are contained within the article and Supplementary Materials.

Conflicts of Interest: The authors declare no conflict of interest.

References

1. Gligorovski, S.; Strekowski, R.; Barbati, S.; Vione, D. Environmental Implications of Hydroxyl Radicals (•OH). *Chem. Rev.* **2015**, *115*, 13051–13092.
2. Mahbub, P.; Duke, Mi. Scalability of Advanced Oxidation Processes (AOPs) in Industrial Applications: A Review. *J. Environ. Manag.* **2023**, *345*, 118861.
3. Li, X.; Luo, R.; Liang, X.; Wu, Q.; Gong, C. Recent Advances in Enhancing Reactive Oxygen Species Based Chemodynamic Therapy. *Chinese Chem. Lett.* **2022**, *33*, 2213–2230.
4. Chen, D.; Xu, Q.; Wang, W.; Shao, J.; Huang, W.; Dong, X. Type I Photosensitizers Revitalizing Photodynamic Oncotherapy. *Small* **2021**, *17*, 2006742.
5. Khan, H.; Shah, M. U. H. Modification Strategies of TiO_2-Based Photocatalysts for Enhanced Visible Light Activity and Energy Storage Ability: A Review. *J. Environ. Chem. Eng.* **2023**, *11*, 111532.
6. Abdurahman, M. H.; Abdullah, A. Z.; Shoparwe, N. F. A Comprehensive Review on Sonocatalytic, Photocatalytic, and Sonophotocatalytic Processes for the Degradation of Antibiotics in Water: Synergistic Mechanism and Degradation Pathway. *Chem. Eng. J.* **2021**, *413*, 127412.
7. Qiu, P.; Park, B.; Choi, J.; Thokchom, B.; Pandit, A. B.; Khim, J. A Review on Heterogeneous Sonocatalyst for Treatment of Organic Pollutants in Aqueous Phase Based on Catalytic Mechanism. *Ultrasonics Sonochem.* **2018**, *45*, 29–49.
8. Wang, X.; Zhong, X.; Gong, F.; Chao, Y.; Cheng, L. Newly Developed Strategies for Improving Sonodynamic Therapy. *Mater. Horiz.* **2020**, *7*, 2028–2046.
9. He, Z.; Du, J.; Miao, Y.; Li, Y. Recent Developments of Inorganic Nanosensitizers for Sonodynamic Therapy. *Adv. Healthcare Mater.* **2023**, *12*, 2300234.
10. Yang, Y.; Wang, X.; Qian, H.; Cheng, L. Titanium-Based Sonosensitizers for Sonodynamic Cancer Therapy. Appl. Mater. Today **2021**, 25, 101215.
11. Maleki, A.; Seyedhamzeh, M.; Yuan, M.; Agarwal, T.; Sharifi, I.; Mohammadi, A.; Kelicen-Uğur, P.; Hamidi, M.; Malaki, M.; Al Kheraif, A. A.; Cheng, Z.; Lin, J. Titanium-Based Nanoarchitectures for Sonodynamic Therapy-Involved Multimodal Treatments. *Small* **2023**, *19*, 22062.
12. Priya, M. H.; Madras, G. Kinetics of TiO_2-Catalyzed Ultrasonic Degradation of Rhodamine Dyes. *Ind. Eng. Chem. Res.* **2006**, *45*, 913–921.
13. Khataee, A.; Sheydaei, M.; Hassani, A.; Taseidifar, M.; Karaca, S. Sonocatalytic Removal of an Organic Dye Using TiO_2/Montmorillonite Nanocomposite. *Ultrasonics Sonochem.* **2015**, *22*, 404–411.
14. Khataee, A.; Kayan, B.; Gholami, P.; Kalderis, D.; Akay, S. Sonocatalytic Degradation of an Anthraquinone Dye Using TiO_2-Biochar Nanocomposite. *Ultrasonics Sonochem.* **2017**, *39*, 120–128.
15. Choi, Y.; Lee, D.; Hong, S.; Khan, S.; Darya, B.; Lee, J. Y.; Chung, J.; Cho, S. H. Investigation of the Synergistic Effect of Sonolysis and Photocatalysis of Titanium Dioxide for Organic Dye Degradation. *Catalysts* **2020**, *10*, 500.
16. Xu, D.; Ma, H. Degradation of Rhodamine B in Water by Ultrasound-Assisted TiO_2 Photocatalysis. *J. Clean. Prod.* **2021**, *313*, 127758.
17. Sheikhmohammadi, A.; Asgari, E.; Nourmoradi, H.; Fazli, M. M.; Yeganeh, M. Ultrasound-Assisted Decomposition of Metronidazole by Synthesized TiO_2/Fe_3O_4 Nanocatalyst: Influencing Factors and Mechanisms. *J. Environ. Chem. Eng.* **2021**, *9*, 105844.

 doi:10.20944/preprints202412.0815.v1

18. Jonnalagadda, U. S.; Su, X.; Kwan, J. J. Nanostructured TiO_2 Cavitation Agents for Dual-Modal Sonophotocatalysis with Pulsed Ultrasound. *Ultrasonics Sonochem.* **2021**, *73*, 105530.
19. Deepagan, V. G.; You, D. G.; Um, W.; Ko, H.; Kwon, S.; Choi, K. Y.; Yi, G. R.; Lee, J. Y.; Lee, D. S.; Kim, K.; Kwon, I. C.; Park, J. H. Long-Circulating Au-TiO_2 Nanocomposite as a Sonosensitizer for ROS-Mediated Eradication of Cancer. *Nano Lett.* **2016**, *16*, 6257–6264.
20. Cao, Y.; Wu, T.; Dai, W.; Dong, H.; Zhang, X. TiO_2 Nanosheets with the Au Nanocrystal-Decorated Edge for Mitochondria-Targeting Enhanced Sonodynamic Therapy. *Chem. Mater.* **2019**, *31*, 9105–9114.
21. Li, F.; Pan, Q.; Ling, Y.; Guo, J.; Huo, Y.; Xu, C.; Xiong, M.; Yuan, M.; Cheng, Z.; Liu, M.; Lin, J. Gold–Titanium Dioxide Heterojunction for Enhanced Sonodynamic Mediated Biofilm Eradication and Peri-Implant Infection Treatment. *Chem. Eng. J.* **2021**, *413*, 127412.
22. Zhang, B.; Chen, J.; Cao, Y.; Chai, O. J. H.; Xie, J. Ligand Design in Ligand-Protected Gold Nanoclusters. *Small* **2021**, *17*, 2004381.
23. Yang, Z.; Yang, X.; Guo, Y.; Kawasaki, H. Review on Gold Nanoclusters for Cancer Phototherapy. *ACS Appl. Bio Mater.* **2023**, *6*, 4504–4517.
24. Albright, E. L.; Levchenko, T. I.; Kulkarni, V. K.; Sullivan, A. I.; DeJesus, J. F.; Malola, S.; Takano, S.; Nambo, M.; Stamplecoskie, K.; Häkkinen, H.; Tsukuda, T.; Crudden, C. M. Atomically Precise Gold Nanoclusters: Synthesis, Properties, and Applications. *J. Am. Chem. Soc.* **2024**, *146*, 5759–5780.
25. Kawawaki, T.; Negishi, Y.; Kawasaki, H. Photo/Electrocatalysis and Photosensitization Using Metal Nanoclusters for Green Energy and Medical Applications. *Nanoscale Adv.* **2020**, *2*, 17–36.
26. Hossain, S.; Hirayama, D.; Ikeda, A.; Ishimi, M.; Funaki, S.; Samanta, A.; Kawawaki, T.; Negishi, Y. Atomically Precise Thiolate-Protected Gold Nanoclusters: Current Status of Designability of the Structure and Physicochemical Properties. *Aggregate* **2023**, *4*, e255.
27. Li, S.; Du, X.; Liu, Z.; Li, Y.; Shao, Y.; Jin, R. Size Effects of Atomically Precise Gold Nanoclusters in Catalysis. *Precis. Chem.* **2023**, *1*, 14–28.
28. Kawamura, K.; Hikosou, D.; Inui, A.; Yamamoto, K.; Yagi, J.; Saita, S.; Kawasaki, H. Ultrasonic Activation of Water-Soluble $Au_{25}(SR)_{18}$ Nanoclusters for Singlet Oxygen Production. *J. Phys. Chem. C* **2019**, *123*, 26644–26652.
29. Yagi, J.; Ikeda, A.; Wang, L.-C.; Yeh, C.-S.; Kawasaki, H. Singlet Oxygen Generation Using Thiolated Gold Nanoclusters under Photo- and Ultrasonic Excitation: Size and Ligand Effect. *J. Phys. Chem. C* **2022**, *126*, 19693–19703.
30. Kawamura, K.; Ikeda, A.; Inui, A.; Yamamoto, K.; Kawasaki, H. TiO_2-Supported Au_{144} Nanoclusters for Enhanced Sonocatalytic Performance. *J. Chem. Phys.* **2021**, *155*, 124702.
31. Yan, N.; Xia, N.; Liao, L.; Zhu, M.; Jin, F.; Jin, R.; Wu, Z. Unraveling the Long-Pursued Au_{144} Structure by X-Ray Crystallography. *Sci. Adv.* **2018**, *4*, eaat7259.
32. Didenko, Y. T.; Pugach, S. P. Spectra of Water Sonoluminescence. *J. Phys. Chem.* **1994**, *98*, 9742–9749.
33. Yasui, K. Production of O Radicals from Cavitation Bubbles under Ultrasound. *Molecules* **2022**, *27*, 4788.
34. Beckett, M. A.; Hua, I. Impact of Ultrasonic Frequency on Aqueous Sonoluminescence and Sonochemistry. *J. Phys. Chem. A* **2001**, *105*, 3796–3802.
35. Lei, H.; He, Q.; Wu, M.; Xu, Y.; Sun, P.; Dong, X. Piezoelectric Polarization Promoted Spatial Separation of Photoexcited Electrons and Holes in Two-Dimensional g-C_3N_4 Nanosheets for Efficient Elimination of Chlorophenols. *J. Hazard. Mater.* **2022**, *421*, 126696.
36. Khan, R.; Naveen, M. H.; Abbas, M. A.; Lee, J.; Kim, H.; Bang, J. H. Photoelectrochemistry of Au Nanocluster-Sensitized TiO_2: Intricacy Arising from the Light-Induced Transformation of Nanoclusters into Nanoparticles. *ACS Energy Lett.* **2021**, *6*, 24–32.
37. Shaltiel, L.; Shemesh, A.; Raviv, U.; Barenholz, Y.; Levi-Kalisman, Y. Synthesis and Characterization of Thiolate-Protected Gold Nanoparticles of Controlled Diameter. *J. Phys. Chem. C* **2019**, *123*, 28486–28493.